Article ID: 1006-8775(2016) 02-0208-12

A NOVEL METHOD FOR CALCULATING VERTICAL VELOCITY: A RELATIONSHIP BETWEEN HORIZONTAL VORTICITY AND VERTICAL MOVEMENT

DING Zhi-ying (丁治英)[1, 2], ZHAO Xiang-jun (赵向军)[1, 2], GAO Song (高 松)[3], LUO Ya-li (罗亚丽)[4]

(1. Key Laboratory of Meteorological Disaster, Ministry of Education / Joint International Research Laboratory of Climate and Environment Change / Collaborative Innovation Center on Forecast and Evaluation of Meteorological Disasters, Nanjing University of Information Science and Technology, Nanjing 210044 China; 2. College of Atmospheric Science, Nanjing University of Information Science and Technology, Nanjing 210044 China; 3. Chongqing Institute of Meteorological Sciences, Chongqing 401147 China; State Key Laboratory of Severe Weather, Chinese Academy of Meteorological Sciences, Beijing 100081 China)

Abstract: The present work provides a novel method for calculating vertical velocity based on continuity equations in a pressure coordinate system. The method overcomes the disadvantage of accumulation of calculating errors of horizontal divergence in current kinematics methods during the integration for calculating vertical velocity, and consequently avoids its subsequent correction. In addition, through modifications of the continuity equations, it shows that the vorticity of the vertical shear vector (VVSV) is proportional to $-\omega$, the vertical velocity in p coordinates. Furthermore, if the change of ω in the horizontal direction is neglected, the vorticity of the horizontal vorticity vector is proportional to $-\omega$. When ω is under a fluctuating state in the vertical direction, the updraft occurs when the vector of horizontal vorticity rotates counterclockwise; the downdraft occurs when rotating clockwise. The validation result indicates that the present method is generally better than the vertical velocity calculated by the ω equation using the wet Q-vector divergence as a forcing term, and the vertical velocity calculated by utilizing the kinematics method is followed by the O'Brien method for correction. The plus-minus sign of the vertical velocity obtained with this method is not correlated with the intensity of dBZ, but the absolute error increases when dBZ is >=40. This method demonstrates that it is a good reflection of the direction of the vertical velocity.

Key words: horizontal vorticity; vertical velocity; continuity equation; Q-vector; vorticity of vertical shear vector
CLC number: P435 **Document code:** A
doi: 10.16555/j.1006-8775.2016.02.011

1 INTRODUCTION

The studies on vertical movement could date back to 1940s (Panofsky[1]; Graham[2]; Ballemy[3]; Bannon[4]). The studies of the 1950s-1960s witnessed the thorough investigation on the adaptation when meteorologists became aware of the importance of the vertical movement by identifying the correlation between the dispersion of gravity wave and the convergence/divergence of wind field during adaptation processes. To date, three major methods for calculating the vertical movement have been proposed: kinematics method, solving ω equation, and thermodynamic method (Panofsky[5]; Petterssen[6]; Haltiner et al.[7] ; Lv et al[8]).

The kinematics method, deemed as one of the simplest and the most straightforward methods to solve the vertical movement, solves the vertical movement velocity through continuity equations in pressure coordinates. Since the accumulated errors in this method are relatively large, several correctional methods have been introduced (O'Brien[9]; Lateef[10]; Fankhauser[11]; Smith[12]), with the O'Brien method as the most popular one.

As for the ω equation approach, two types of classical ω equations are usually involved: the quasi-geostrophic ω equation and the balance-mode ω equation. Among the various forcing factors of the ω equation are the differential term on vorticity advection and the Laplacian terms on temperature advection, which are considered to cause the vertical movement of the atmosphere. However, it is usually difficult to qualitatively determine the direction of the vertical movement when the signs of the two abovementioned terms are opposite. That is to say, it is assumed that the differential term on vorticity advection is positive, the Laplacian term on temperature advection is negative, then the former will cause the upward movement, the downward

Received 201 4-11-29; **Revised** 2015-12-22; **Accepted** 2016-04-15
Foundation item: National Key Basic Research Development Program "973" (2013CB430103, 2009CB421503); National Natural Science Funding (41375058, 41530427); State Key Laboratory of Severe Weather, Chinese Academy of Meteorological Sciences (2015LASW-A07)
Biography: DING Zhi-ying, Professor, primarily undertaking research on mesoscale meteorology.
Corresponding author: DING Zhi-ying, e-mail: dingzhiying@nuist.edu.cn

movement caused by the later. Therefore, in the absence of quantitative calculation, it is hard to determine the interaction is upward movement or downward movement. This, along with that a partial offset effect also exists between the two terms, have rendered the use of the traditional ω equation on both quantitative calculation and qualitative applications less desirable. In this regard, Hoskins proposed to turn the quasi-geostrophic forcing term into a vector divergence, and named it Q-vector (Hoskins et al.[13]). The new ω equation, incorporating the Q-vector divergence as the forcing term, has advantages over the traditional approach of including the effects mentioned with one forcing and of Q-vector to be easily solved and even manually estimated. Following the initial Q-vector modification, other Q-vectors, including general Q-vector, semi-geostrophic Q-vector, ageostrophic dry Q-vector and ageostrophic wet Q-vector. have been further proposed and tested, with satisfactory results (Yue and Shou[14]).

The thermodynamic method is an alternative approach to calculate the vertical velocity through the use of the thermodynamic equation. However, this method requires several preconditions, including the variability of the potential temperature and that it has to be at the upper troposphere. Moreover, the potential temperature equilibrium may also cause a relatively large error.

There are also other diagnostic methods to calculate the vertical velocity, including the inverse calculation from precipitation, derivation from topography, and the inverse calculation of vertical movement from radar echoes (Larsen and Rottger[15]; Jagannadha et al.[16]). However, the inverse calculation from precipitation and derivation from topography suffer the limited applications due to the fact that the vertical velocity can only be calculated under specific conditions. And the inverse calculation of vertical movement from radar echoes, one of the most widely applied methods in recent years, partly due to the availability of more data from satellites, is still far from perfect due to certain bias in information retrieved from satellite data.

A large body of studies have shown that the environmental wind vertical shear plays an important role in maintaining severe local convective storm by affecting the type, movement, and dynamic character of the convective storm. Generally speaking, the supercell storm has the strongest wind vertical shear, whereas the normal single-cell storm is the weakest, and the shear of the multi-cell storm lies in between. Many field observations have revealed that almost all single-cell and multi-cell storms occur with strong wind shear (Browning and Foote[17]; Fankhauser[18]). Marwitz[19] noticed that a supercell storm generally occurs at a wind shear speed of from $2.5\cdot10^{-3}$ to $4.5\cdot10^{-3}s^{-1}$. In studying the influence of vertical distribution on vertical movement field dur ing a diabatic heating process, Pan and Chen[20] found that the vertical velocity would generally increase when the parameter of zonal wind vertical shear speed increases. Wu et al.[21] found that different vertical wind shears have different effects on the development and evolve ment of convective storms. Further, Yang and Jian[22] proposed that there is a certain mutual adaptation between the vertical movement field and vertical shear field by researching the developments and roles of the vertical wind shear in convective storms. It can be summarized from the report above that there is an undoubted relationship between vertical wind shear and vertical movement. However, all the aforementioned studies only showed observational understandings of the roles of vertical wind shear in the development of convective storms and the relationship between vertical wind shear and vertical movement, and we are still in lack of the theoretical relationship between the vertical shear and vertical velocity. To address this issue, the present work, for the first time, reports the theoretical relationship between vertical wind shear and vertical movement based on continuity equations in pressure coordinates, and proposes a novel method for calculating the vertical velocity by applying this correlation.

2 RELATIONSHIP BETWEEN HORIZONTAL VORTICITY AND VERTICAL MOVEMENT

2.1 *Relationship between mesoscale system and hydrostatic equilibrium*

An atmospheric circulation contains kinematic systems of various scales, from turbulent micelle to superlong wave. The physical properties of kinematic systems of different scales are quite different. For the convenience of our research they should be classified. There are various classification methods for kinematic systems. According to the comprehensive analysis results of observation and theory, Orlanski[23] proposed a detailed scales division scheme which was widely used. According to his scheme, weather systems can roughly be divided into three categories, i.e., the large scale, the mesoscale and the small scale. The large scale systems can be sub-grouped into two categories: α and β. The mesoscale and small scale systems can be classified into three types, respectively: α, β and γ. In accordance with this classification method, the mesoscale is a wide range (i.e., 2 to 2 000 km) category which includes small systems (such as thunderstorm cell, etc) and big systems that are usually called weather systems (such as fronts, typhoons, hurricanes, etc). Its main components are systems from 20 to 200 km, namely the β mesoscale systems. The β mesoscale systems have the typical features of mesoscale systems. An analysis of the relative importance for the Coriolis force and buoyancy shows that the large mesoscale movement can be quasi-geostrophic and quasi-hydrostatic balanced movement while the small mesoscale movement can be ageostrophic and non-hydrostatic balanced movement. At the same time, the typical mesoscale movement may be ageostrophic and quasi-hydrostatic balanced movement. According to the scale analysis method (Charney[24]), taking the order of

magnitude of horizontal wind speed as V~10 m/s, the order of magnitude of vertical scale as H~ 10^4 km, for α, β and γ mesoscale systems, the order of magnitude of vertical velocity is 10^{-1}, 10^0, 10^1 m/s, respectively. The order of magnitude of each term of the vertical movement equation for the α, β and γ mesoscale systems at a certain latitude can be estimated through the above characteristic scale. Taking β mesoscale as an example, the vertical movement is

$$\frac{dw}{dt}=-\frac{1}{\rho}\frac{\partial p}{\partial z}+2\Omega u\cos\varphi-g+F_z$$

and the scale of each term is $\frac{VW}{L}$, $\frac{P_0}{\rho H}$, f_0V, g, and $\frac{\nu W}{H^2}$, respectively, and the order of magnitude is 10^{-3}, 10, 10^{-3}, 10, and 10^{-12}, respectively.

For simplicity, assuming that the system center is located at latitude where φ=45^0, hence $f_0\cong10^{-4}$s^{-1}. Because the pressure decreases by about one order of magnitude from the ground to the troposphere, the scale of the vertical pressure gradient is set as P_0/H, where P_0 is the pressure at the ground. In addition, the order of magnitude of ρ is set as 1 kg/m^3. ν is the kinematic viscosity coefficient. $\nu\cong10^{-5}$m^2/s. g is the acceleration of gravity. Ω is the angular velocity of earth rotation.

It can be seen that the hydrostatic equilibrium is basically existent within the scope of the mesoscale. Even in the γ mesoscale, the order of magnitude of $\frac{dw}{dt}$ can only reach 10^{-1}m/s^2, which basically meet the need of the hydrostatic equilibrium. Therefore, except for the very small scale systems, such as tornadoes and deep convection, which may not be able to fully satisfy the hydrostatic equilibrium conditions, hydrostatic equilibrium relationship can be applied to most of the weather systems of different scales. Currently, most scholars also believe that the β mesoscale system satisfies the quasi-hydrostatic equilibrium conditions.

2.2 *Deduction of principle of relationship between horizontal vorticity and vertical movement*

To avoid the accumulation of errors due to the integration of divergences in the kinematics method, a novel method for calculating vertical velocity using continuity equations has been proposed.

The continuity equation in p coordinates is expressed as

$$\left(\frac{\partial u}{\partial x}+\frac{\partial v}{\partial y}\right)_p+\frac{\partial\omega}{\partial p}=0 \tag{1}$$

Take partial derivative of Eq.(1) with respect to p and obtain

$$\frac{\partial}{\partial x}(-\frac{\partial u}{\partial p})-\frac{\partial}{\partial y}(\frac{\partial v}{\partial p})=\frac{\partial^2\omega}{\partial p^2} \tag{2}$$

And the three-dimensional vorticity in z coordinates is

$$\xi=\vec{i}\left(\frac{\partial w}{\partial y}-\frac{\partial v}{\partial z}\right)+\vec{j}\left(\frac{\partial u}{\partial z}-\frac{\partial w}{\partial x}\right)+\vec{k}\left(\frac{\partial v}{\partial x}-\frac{\partial u}{\partial y}\right) \tag{3}$$

Hence, the horizontal vorticity in z coordinates can be written as

$$(\xi_x,\xi_y)=(\frac{\partial w}{\partial y},-\frac{\partial w}{\partial x})+(-\frac{\partial v}{\partial z},\frac{\partial u}{\partial z})=(\xi_{x1},\xi_{y1})+(\xi_{x2},\xi_{y2}) \tag{4}$$

The gradient of vertical velocity in the horizontal direction is denoted as $\nabla w=(\frac{\partial w}{\partial x},\frac{\partial w}{\partial y})$. For the updraft, ∇w points to the center of the vertical movement; for the downdraft, ∇w points to the edge of the vertical movement. Meanwhile,

$$(\xi_{x1},\xi_{y1})=(\frac{\partial w}{\partial y},-\frac{\partial w}{\partial x})=\nabla w\times\vec{k} \tag{5}$$

Therefore, according to the right-hand rule of cross product, vector (ξ_{x1},ξ_{y1}) rotates counterclockwise in the area of updraft but clockwise in the area of downdraft. This phenomenon exists in both the hydrostatic equilibrium and the non-hydrostatic equilibrium conditions.

Meanwhile, according to the P–Z coordinate transformation based on the hydrostatic equilibrium relationship and the state equation, it can be obtained that

$$\frac{\partial v}{\partial z}=-\frac{pg}{RT}\cdot\frac{\partial v}{\partial p};\ \frac{\partial u}{\partial z}=-\frac{pg}{RT}\cdot\frac{\partial u}{\partial p} \tag{6}$$

Therefore, the expression of the horizontal vorticity is

$$-\frac{\partial v}{\partial z}=\frac{pg}{RT}\cdot\frac{\partial v}{\partial p}=\xi_{x2};\ \frac{\partial u}{\partial z}=-\frac{pg}{RT}\cdot\frac{\partial u}{\partial p}=\xi_{y2} \tag{7}$$

wherein ξ_{x2} and ξ_{y2} are the component in the i and j direction of the horizontal vorticity, respectively. The following can be obtained from Eq.(7):

$$-\frac{\partial v}{\partial z}\propto\frac{\partial v}{\partial p}\propto\xi_{x2}\ ;\ \ \frac{\partial u}{\partial z}\propto-\frac{\partial u}{\partial p}\propto\xi_{y2} \tag{8}$$

The last term in Eq.(3) represents the rotation of horizontal wind velocity (u,v) in the horizontal direction. The vorticity has a plus sign when horizontal wind velocity rotates counterclockwise, and a minus sign when the said velocity rotates clockwise. Therefore, $\frac{\partial v}{\partial p}$ in Eq.(2) is equivalent to the u component of vertical vorticity in Eq.(3), $-\frac{\partial u}{\partial p}$ is equivalent to the v component, and the left-hand side of Eq.(2) can be considered as the rotation of vertical shear $(\frac{\partial v}{\partial p},-\frac{\partial u}{\partial p})$ of horizon-

tal wind in the horizontal direction. Since the only difference between $(\frac{\partial v}{\partial p}, -\frac{\partial u}{\partial p})$ and $(\xi_{x2}, \xi_{y2}) = (\frac{pg}{RT} \cdot \frac{\partial v}{\partial p}, -\frac{pg}{RT} \cdot \frac{\partial u}{\partial p})$ is one factor $\frac{pg}{RT}$, the horizontal vorticity (ξ_{x2}, ξ_{y2}) has the same rotation with the vertical shear $(\frac{\partial v}{\partial p}, -\frac{\partial u}{\partial p})$ of horizontal wind in the horizontal direction. Furthermore, when ω field is under fluctuating state, $\frac{\partial^2 \omega}{\partial p^2} \propto -\omega$. Therefore, the present article obtained the following relationship of horizontal vorticity and vertical movement: when the horizontal vorticity $(\frac{\partial v}{\partial p}, -\frac{\partial u}{\partial p})$ vector rotates counterclockwise, the vector has a plus sign, then $\omega<0$, accompanying the occurrence of an updraft; when the horizontal vorticity $(\frac{\partial v}{\partial p}, -\frac{\partial u}{\partial p})$ vector rotates clockwise, the vector has a minus sign, then $\omega>0$, and a downdraft exists. The 200 hPa vector-graphs of $(\frac{\partial v}{\partial p}, -\frac{\partial u}{\partial p})$ at 13:00 on 19 June 2010 calculated via WRF output fields are shown in Fig. 1. The shadowed area represents the vertical velocity obtained from WRF output fields. The data of vertical velocity is transformed through $\omega \approx -\rho g w$, thus the unit is Pa s^{-1}. The shadowed part denotes either an updraft or a downdraft. It can be seen that the horizontal vorticity vector rotates counterclockwise at the negative value center, and rotates clockwise at the positive value center.

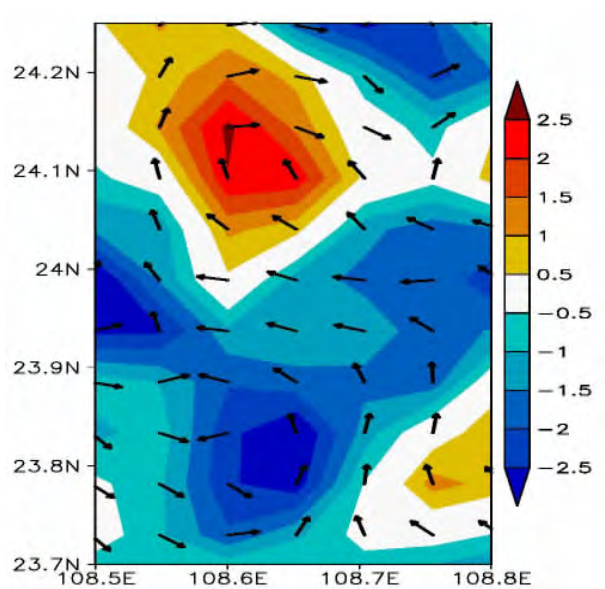

Figure 1. Vectorgraph of horizontal wind vertical shear $(\frac{\partial v}{\partial p}, -\frac{\partial u}{\partial p})$ at 200 hPa (Units: 10^{-3} m s^{-1} Pa^{-1}). The shadowed area represents the vertical velocity (Unit: Pa s^{-1}).

The above analysis indicates that both (ξ_{x1}, ξ_{y1}) and (ξ_{x2}, ξ_{y2}) rotate counterclockwise when it is updraft. Accordingly, the horizontal vorticity (ξ_x, ξ_y) also rotates counterclockwise. Both (ξ_{x1}, ξ_{y1}) and (ξ_{x2}, ξ_{y2}) rotate clockwise when it is downdraft. For that reason, the horizontal vorticity (ξ_x, ξ_y) also rotates clockwise. In general, however, a closed circulation of vector (ξ_{x2}, ξ_{y2}) can form only when the vertical velocity is near its extremum area in the vertical direction, while a closed circulation of vector (ξ_{x1}, ξ_{y1}) can form as long as it is near the center of the vertical movement in the horizontal direction. According to the scale analysis, the vertical velocity is much smaller than the horizontal velocity within the scope of $\alpha \sim \beta$ mesoscale, i.e., the effect of (ξ_{x1}, ξ_{y1}) is far smaller than (ξ_{x2}, ξ_{y2}). (ξ_{x1}, ξ_{y1}) is more important than (ξ_{x2}, ξ_{y2}) only when the horizontal shear of the vertical velocity is far greater than the vertical shear of the horizontal wind (in small scale or γ mesoscale systems), such as in the conceptual model of microburst proposed by Fujita[25].

2.3 *Calculation of vertical velocity*

As described above, the vertical shear $(\frac{\partial v}{\partial p}, -\frac{\partial u}{\partial p})$ of the horizontal wind and the horizontal vorticity (ξ_{x2}, ξ_{y2}) have the same rotation direction in horizontal direction. For the convenience of the descriptions below, we call $\frac{\partial}{\partial x}(-\frac{\partial u}{\partial p}) - \frac{\partial}{\partial y}(\frac{\partial v}{\partial p})$ the vorticity of the horizontal vorticity and label it as ξ, i. e., Eq.(2) is the Poisson's equation. The vertical velocity can be obtained through solving Eq. (2) by iteration using relaxation method.

3 VALIDATION ASSESSMENT

We herein analyze the reliability as well as the pros and cons of this new method by comparing the vertical velocity obtained in this work through solving equation Eq.(2) with ω calculated using the other three methods. The ω (as the unit of vertical velocity obtained from the output of WRF is m/s, the data is transformed through $\omega \approx -\rho g w$. Except for the contrary sign to w, there is only numerical error for the vertical velocity in p coordinates obtained through this transformation) obtained from the output of the non-hydrostatic equilibrium mode of WRF is herein labeled as ω_{wrf}. The corrected vertical velocity through kinematics method and O'Brien method, calculated using the horizontal wind velocity u and v obtained from the model output is labeled as ω_{ob}. The vertical velocity solved from the ω equation using wet Q-vector divergence as forcing term is labeled as ω_{qv} (Gao [26]). The ω equation using wet Q-vector divergence used in this article is as follows.

$$\nabla^2(\sigma\omega) + f^2 \frac{\partial^2 \omega}{\partial p^2} = -2\nabla \cdot Q^* \quad (9)$$

wherein, $\sigma = -h\frac{\partial \theta}{\partial p}$, $h = \frac{R}{P}(\frac{P}{1000})^{R/C_p}$, f is the Coriolis parameter.

$$Q_x^* = \frac{1}{2}[f(\frac{\partial v}{\partial p}\frac{\partial u}{\partial x} - \frac{\partial u}{\partial p}\frac{\partial v}{\partial x}) - h\frac{\partial V}{\partial x}\cdot\nabla\theta - \frac{\partial}{\partial x}(\frac{LR\omega}{C_p\cdot p}\frac{\partial q_s}{\partial p})] \quad (10)$$

$$Q_y^* = \frac{1}{2}[f(\frac{\partial v}{\partial p}\frac{\partial u}{\partial y} - \frac{\partial u}{\partial p}\frac{\partial v}{\partial y}) - h\frac{\partial V}{\partial y}\cdot\nabla\theta - \frac{\partial}{\partial y}(\frac{LR\omega}{C_p\cdot p}\frac{\partial q_s}{\partial p})] \quad (11)$$

where the $-2\nabla\cdot Q^*$ at the right-hand side of Eq.(9) can be solved by taking ω_{wrf} into Eqs.(10) and (11), and the vertical velocity ω_{qv} can be obtained iteratively using the relaxation method.

The initial data for running WRF mode were 1°×1° 6-hour global final analysis data (FNL) from the National Centers for Environmental Prediction (NCEP) and the National Center for Atmospheric Research (NCAR). The model utilized a triple nested simulation method over the [20°N, 40°N; 101°E, 124°E] region on a 444×396 grid with a grid interval of 4 km. The model simulated deep convection and rainstorm in a MCC from 0000 Universal Time Coordinate (UTC) 19 June to 1200 UTC 20 June 2010. For the distribution of radar echo in Fig.2, it can be seen that although the simulated echo (Fig.2a) is further south than the observed one (Fig.2b), the simulated echo orientation agrees well with the actual orientation, both with the northeast-southwest direction; and the temporal evolution of the simulated echo agrees well with that of the actual echo, both moving to the south of Guangxi and stretching toward its northwest; and the strength of the multiple strong echo centers of the simulated echo belt is also consistent with that of the radar echo. Therefore, the output result of this simulation can serve as a comparison basis for the assessment of this work.

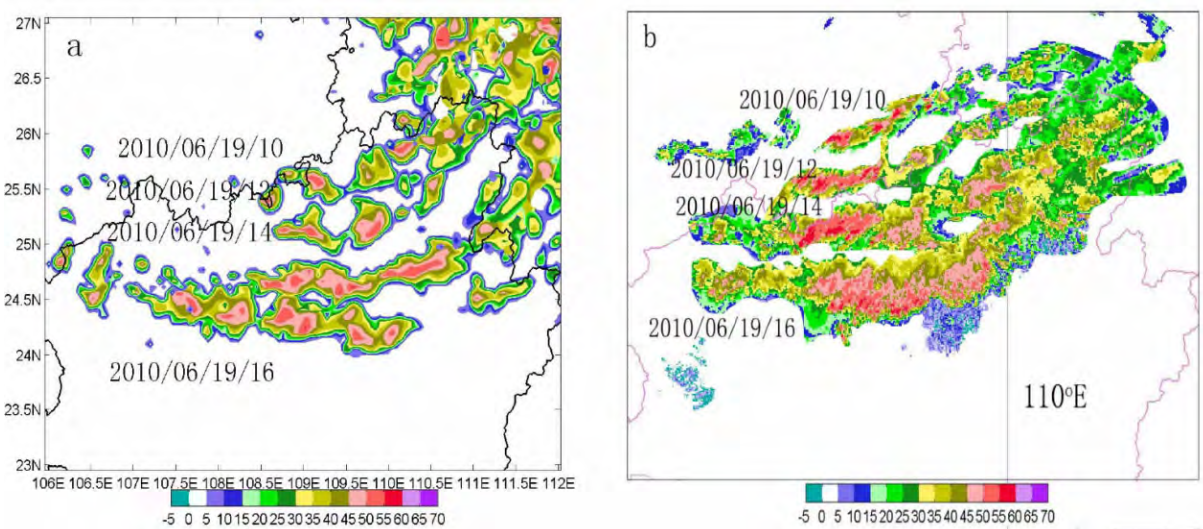

Figure 2. (a) Simulated and (b) observed radar echo distributions from 1000 UTC on 19 June to 1600 UTC on 19 June 2010 (Units: dBZ).

Figure 3 shows the temporal evolution of the strongest upward and downward draft of each level. It can be seen that the strongest vertical movement occurs between 1000 UTC and 1600 UTC 19 June 2010. The strongest updraft velocity is more than 30 m/s at roughly 200 hPa; the strongest downdraft has two centers, one near 200 hPa, the other in proximity of 700 hPa; the maximum downdraft velocity reaches approximately 10 m/s. It shows that this process has obvious mesoscale features. It needs further verification to determine whether the vertical movement with mesoscale features can be solved with Eq.(2).

Figure 4 shows the vertical velocity fields at 1300 UTC on 19 June 2010 at varying levels obtained with the four methods. It can be seen from the figure that each field has an overall good consistency. Specifically, at the middle level (Figs.4 (a2, b2, c2, and d2)), the vertical movements obtained with each method are surprisingly similar, whereas a remarkable difference can be observed between the ω_{qv} and other vertical velocity fields at the low and high levels. However, the positions of positive and negative zones and central intensities of the ω_{qv} are much close to those obtained with other methods, and therefore, the comparisons of orientation consistency and absolute errors can be performed. The vertical velocity (ω_{wrf}) in WRF is obtained by considering influences of factors such as non-hydrostatic equilibrium, various forms of water vapor and friction force. Therefore, the vertical velocity calculated with this method is more reasonable as compared to that obtained through other quasi-hydrostatic equilibrium-based methods, thus justifying our comparison of the vertical velocities obtained through the other three methods to the ω_{wrf}.

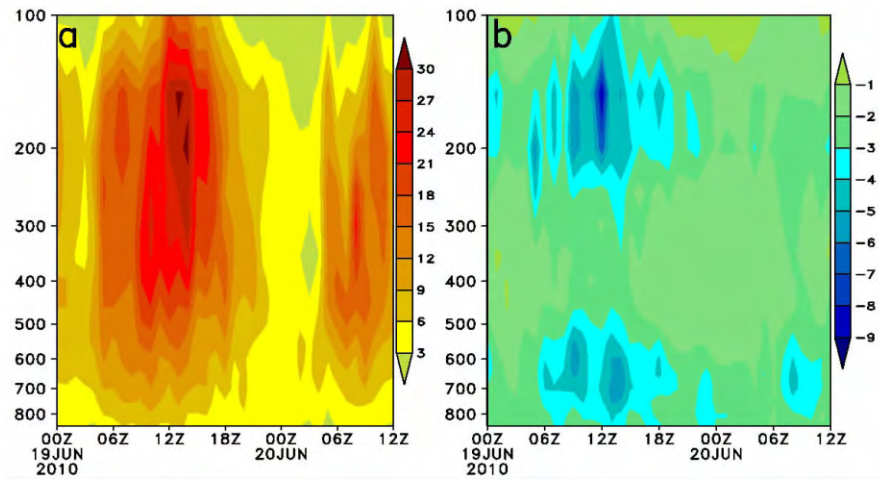

Figure 3. Temporal evolution of the strongest updraft (a) and the strongest downdraft (b) at each level (Units: m s^{-1}).

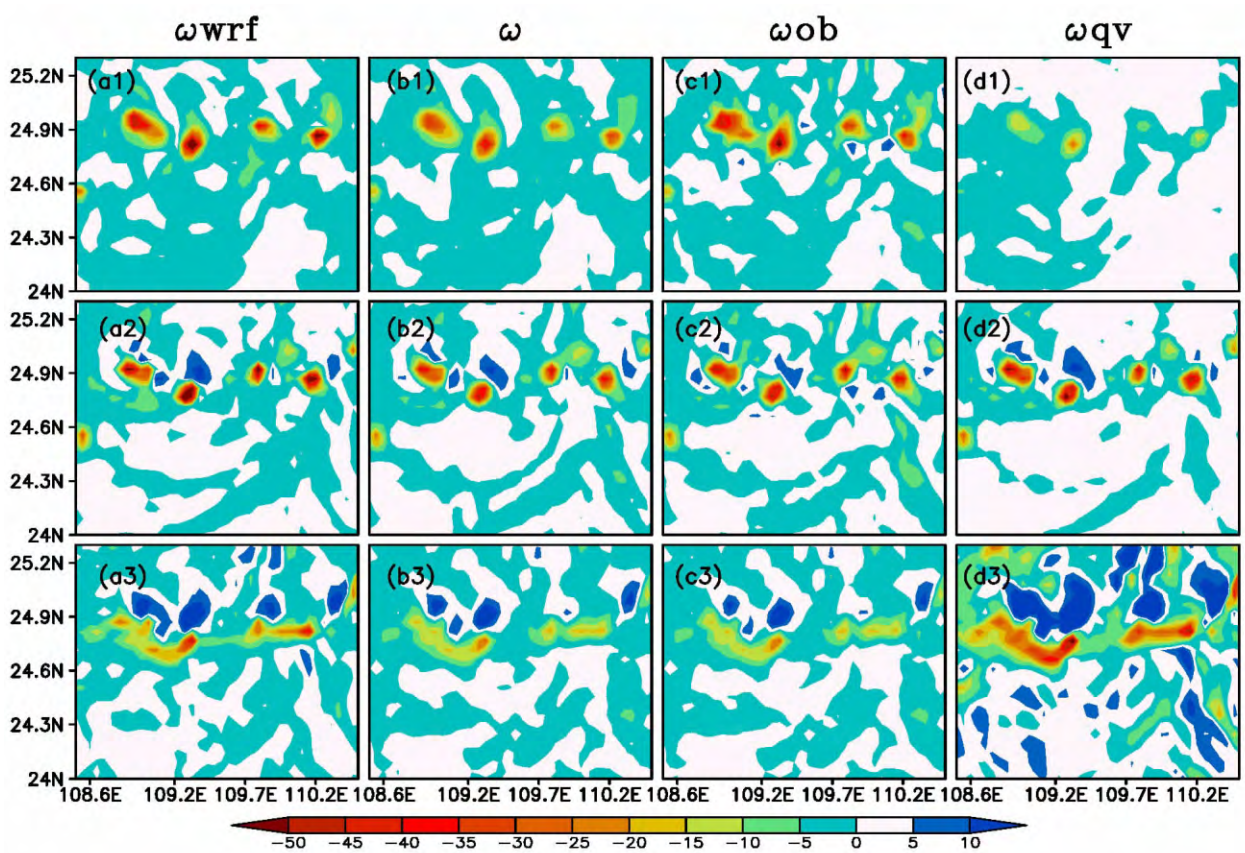

Figure 4. 200, 500 and 800 hPa ω fields (a1-a3), ω_{ob} fields (b1-b3), ω_{wrf} fields (c1-c3), and ω_{qv} field (d1-d3). Units: Pa s^{-1}.

Next, we will assess the validation of the method disclosed herein in two aspects. First, we will validate the method by separately assessing the plus-minus consistency percentage ratio between the vertical velocities calculated with the three methods and the vertical velocity obtained from the WRF diagnosis. Second, we are to validate the method by assessing the absolute errors between the vertical velocities calculated with the three methods and the vertical velocity obtained from the WRF diagnosis.

3.1 *Plus–minus consistency assessment*

To validate the method by assessing the plus-minus consistency between the vertical velocities calculated with the three methods and the vertical velocity obtained from the WRF diagnosis, the percentage ratios of the coverage of the amount of grid blocks, which are plus-minus consistency between the vertical velocity calculated with each method and the vertical velocity obtained from the WRF diagnosis, to the total amount of plus-minus grid blocks within simulation region were

compared, in order to objectively demonstrate the ability of this method on vertical velocity calculation. The expression is shown below.

$$GP=\sum G_i / \sum Gwrf_i \times 100\% \quad (12)$$

wherein $\sum G_i$ is the total amount of grid blocks plus-minus consistency between any method and ω_{wrf} within the same space, and $\sum Gwrf_i$ is the total amount of plus-minus grid blocks in ω_{wrf}.

To better illustrate the plus-minus consistency between the vertical velocities obtained with three methods and the vertical velocity from WRF diagnosis, and to determine whether there were differences between the consistency percentage ratios from strong and weak convective zones within the same level, the simulation region was therefore divided into areas according to dBZ intensity, and the plus-minus consistency was then calculated for each area. This article divided the dBZ into the following intervals (0,10] (i. e., 0<dBZ≤10, hereinafter the same), (10,20], (20,30], (30,40] , (40,∞).

Figure 5 is the GP of ω, ω_{ob} and ω_{qv} at each integral time and within each dBZ range. In this figure, within 0-10 dBZ range (Fig.5a), the plus-minus consistency at 850 hPa was approximately 80%, 550 hPa had less variance and had a plus-minus consistency of approximately 75%, and the plus-minus consistency at 250 hPa was approximately 85%; within 10-20 dBZ range (Fig.5b), the consistencies at 850 and 550 hPa were similar to those of within the 0-10 dBZ range. However, on average, the consistency at high levels increased to approximately 95%. As dBZ increased, there were also increases of plus-minus consistency at high levels (Fig. 5c-e) and consistency at middle levels, and there was also a slight increase of consistency at low levels, wherein within the range of more than 40 dBZ, the consistencies were generally maintained at over 80% at low levels, over 90% at middle levels, and almost 100% at high levels.

In Fig.5a1-e1, the GP variation trends of ω_{ob} at each dBZ range and at 850 hPa, 550 hPa and 250 hPa level were generally consistent with those in Fig. 5 (a-e). However, the GP of ω_{ob} at each dBZ range was lower than the corresponding GP of ω at each dBZ range at 250 hPa level, and the GP of ω_{ob} at each dBZ range was slightly lower than the GP of ω at each dBZ range at the 850 and 550 hPa levels.

For the GP variation trends of ω_{qv} at each dBZ range and at 850, 550 and 250 hPa (Fig.5a2-e2), the results are also generally consistent with those in Fig. 5a-e. The difference was as follows: at the 850 and 550 hPa levels, the GP of ω_{qv} at each dBZ range was higher than the corresponding GP of ω at each dBZ range, and at the 250 hPa level, the GP of ω_{qv} was lower than the GP of ω at each dBZ range.

It can be known from the above analysis that at 850 hPa and 550 hPa, the GP of ω_{qv} at each dBZ range was higher than those in ω and ω_{ob}; at 850 hPa, the GP of ω within each dBZ range was generally consistent with the GP of ω_{ob} within each dBZ range; at 550 hPa, the GP of ω at each dBZ range was higher than those in ω_{ob}; at 250 hPa, accompanied with the increasing dBZ, the GPs under the three methods all increased and were close to 100%; however, the method disclosed herein is closest to ω_{wrf}. Overall speaking, the higher the dBZ was, the higher the plus-minus consistency would be.

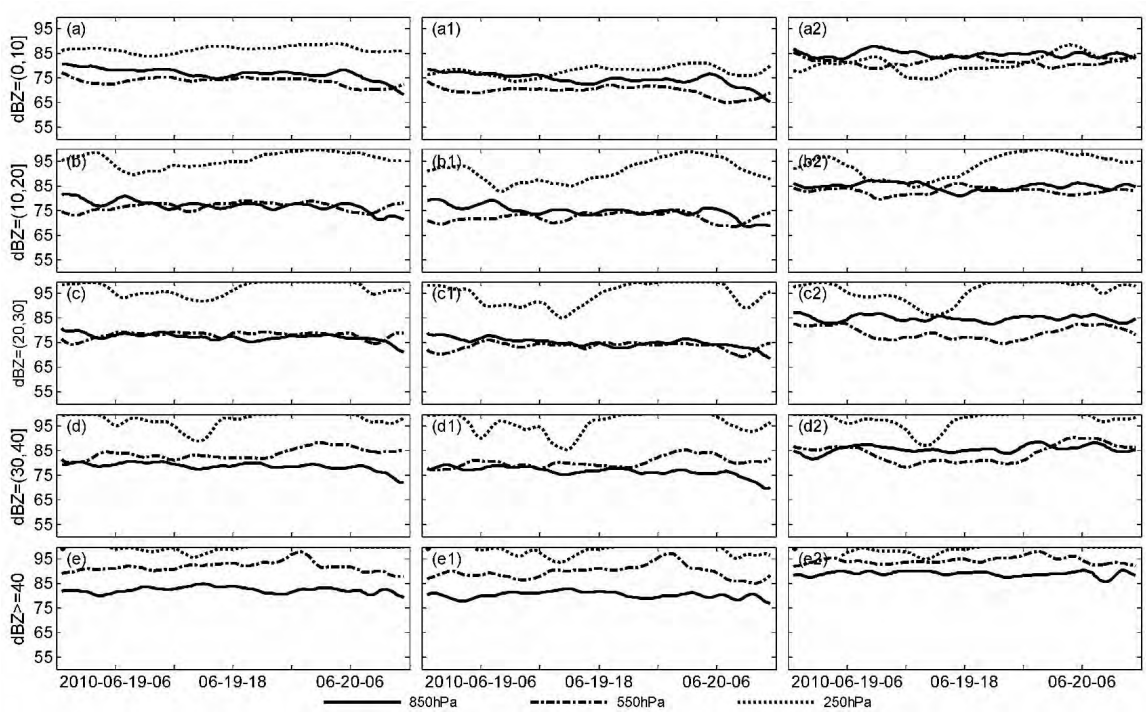

Figure 5. ω (a-e), ω_{ob} (a1-e1), ω_{qv} (a2-e2) GP within each dBZ range, at each time point and at 850, 550 and 250 hPa levels. Units: %.

3.2 *Absolute error assessment*

The conclusion of plus-minus consistency provided in Section 3.1 indicates that the diagnosed upward and downward movement by the method disclosed herein were well consistent with that diagnosed by WRF, and that the method disclosed herein was remarkably better than the ω_{qv} and ω_{ob} methods at the high level. However, in investigating the vertical movement, both its direction and the intensity of the upward and downward movement should be considered. Therefore, the assessment on plus-minus consistency was not adequate to demonstrate that the method disclosed herein on the calculation of vertical velocity was more effective, and the differences between values of ω and ω_{wrf} should also be considered. The specific assessment strategies were shown below:

(1) Since significant differences exist between the intensity of vertical movement of the convective and non-convective zone, similar to the plus-minus consistency assessment in Section 3.1, the dividing of the region according to the intensity of dBZ was also required in this section;

(2) Solve the individual average upward and downward velocity at each level within each dBZ interval, divide the atmosphere into three levels, i. e., the high, middle, and low levels, and calculate the average downward (upward) velocity at these three levels and within each dBZ range. Specifically, the atmosphere is divided as follows: with a 50 hPa interval, there are totally 14 levels from 850 hPa to 200 hPa (due to the terrain influence at the low level, there were many default values, and therefore, the lowest level was set to be at 850 hPa). The average vertical velocity at 850-650 hPa is labeled as *ave*_L, that of at 600-400 hPa as *ave*_M, and that of at 350-200 hPa as *ave*_H; for any dBZ interval, the average downward (upward) velocity within a defined region of the dBZ interval is calculated at each of the low, middle, and high levels.

Respectively, label the average vertical velocities within a defined region of any dBZ interval at the high, middle and low levels, which are determined by taking ω and ω_{wrf} into steps (1) and (2), as ave_H_ω, ave_M_ω and ave_L_ω; ave_H_ω_{wrf}, ave_M_ω_{wrf} and ave_L_ω_{wrf}. Therefore, the absolute errors at the high, middle, and low levels are respectively:

abserr_H=ave_H_ω- ave_H_ω_{wrf};

abserr_M= ave_M_ω- ave_M_ω_{wrf};

abserr_L= ave_L_ω- ave_L_ω_{wrf}.

The absolute errors of ω_{qv}, ω_{ob} and ω_{wrf} were also labeled in the similar manner.

At the low level and within the (0, 10] dBZ interval (Fig. 6a), the ave_L_ω and ave_L_ω_{wrf} were relatively close to each other, and the abserr_L were mostly 0 with the values thereof fluctuated within 0-0.25 Pa/s. Within (10, 20] and (20, 30] dBZ intervals (Fig.6b-c), the ave_L_ω and ave_L_ω_{wrf} exhibited little difference between the duo, the abserr_L was fluctuated around 0.5 Pa/s, and the average value of the updraft was approximately -2 Pa/s. Corresponding to the increasing of dBZ (Fig.6d), the absolute values of ave_L_ω and ave_L_ω_{wrf} also slightly increased, the abserr_L was fluctuated around 1 Pa/s, and the upward velocity was increasing from 2 Pa/s to approximately 3 Pa/s; when dBZ>=40 (Fig.6e), the values of ave_L_ω and

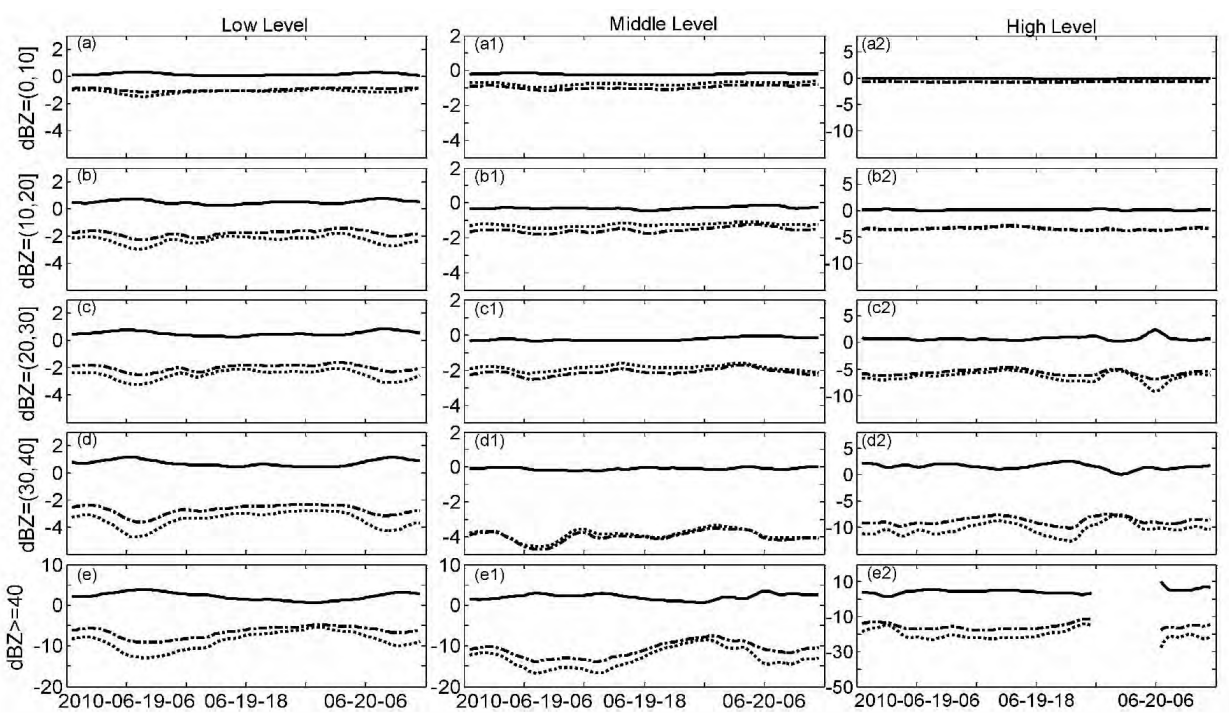

Figure 6. The average upward velocities of ω (dot-dash line) and ω_{wrf} (dotted line) at each time point within dBZ intervals at the low (a to e), middle (a1 to e1), and high (a2 to e2) levels, and the absolute errors (solid line) between the two. Units: Pa s^{-1}.

ave_L_ω_{wrf} exhibited a significant increase (approximately -7.5 Pa/s); nevertheless, the two were still remarkably close to each other, with the abserr_L fluctuated around 2 Pa/s. In general, the higher the dBZ was, the larger the absolute error caused by upward movement was, though the relative error exhibited less increase.

At the middle level, as shown in Fig.6a1-e1, at each dBZ interval, the fluctuation range and the change trends of ave_M_ω, ave_M_ω_{wrf} and abserr_M were generally the same as those of shown in Fig.6a-e. The difference was as follows. The absolute value of ave_M_ω was larger than ave_M_ω_{wrf}, the abserr_M was fluctuated within the range of 0 to -0.5 Pa/s (Fig. 6a1-d1), and when dBZ>=40, the abserr_M was fluctuated around 2 Pa/s. However, the smallest absolute error fell into the (30,40] dBZ interval.

At the high level, as shown in Fig.6a2-e2, within the (0,20] dBZ interval, the absolute error was almost 0 and gradually increased as dBZ went above 20.

The analysis above suggests as follows. For the updraft, at the low, middle, and high levels and within each dBZ interval, the values of ω and ω_{wrf} exhibited good consistency, and the following can be observed. Within each dBZ interval, the absolute value of ω was slightly smaller than the absolute value of ω_{wrf} at the low and high levels; the absolute value of ω was slightly larger than the absolute value of ω_{wrf} at the middle level. In general, the absolute error was small within the (0,20] dBZ interval, and the absolute error was relatively large when dBZ went above 40, though the relative error exhibited less change.

The same calculation was done to obtain the following: in the case of the downdraft (figure not shown), at low, middle and high levels, the values of ω and ω_{wrf} also exhibited good consistency, and it can also be observed that: within each dBZ interval, the ω was slightly smaller than ω_{wrf} at the low level; the ω was slightly larger than ω_{wrf} at the middle level.

The results of aforementioned plus-minus consistency and absolute error assessments suggest that the vertical velocity ω, calculated by the method disclosed herein and the vertical velocity ω_{wrf} output by WRF, exhibited good consistency in terms of upward/downward movement consistency and vertical movement intensity.

To further assess the method disclosed herein, ω, ω_{ob}, ω_{qv} and ω_{wrf} were separately subjected to the above assessment steps to obtain the absolute errors of average upward vertical velocities of ω, ω_{ob}, ω_{qv} and ω_{wrf} at each of the low, middle, and high levels in the defined region of any dBZ interval. By examining three types of absolute error, we are able to determine pros and cons of each method.

At the low level, it was shown in Fig.7a-e that except for the (0,10] dBZ, the absolute errors of the ave_L_ω, ave_L_ω_{ob} with respect to the ave_L_ω_{wrf} were generally overlapped and were above 0; the absolute value of absolute error between ave_L_ω_{qv} and ave_L_ω_{wrf} was significantly larger than the other two absolute errors and the absolute error was generally below 0; it was obvious that the absolute error of the vertical velocity at the low level calculated through the wet Q-vector was the largest.

At the middle level, as shown in Fig.7a1-e1, on av-

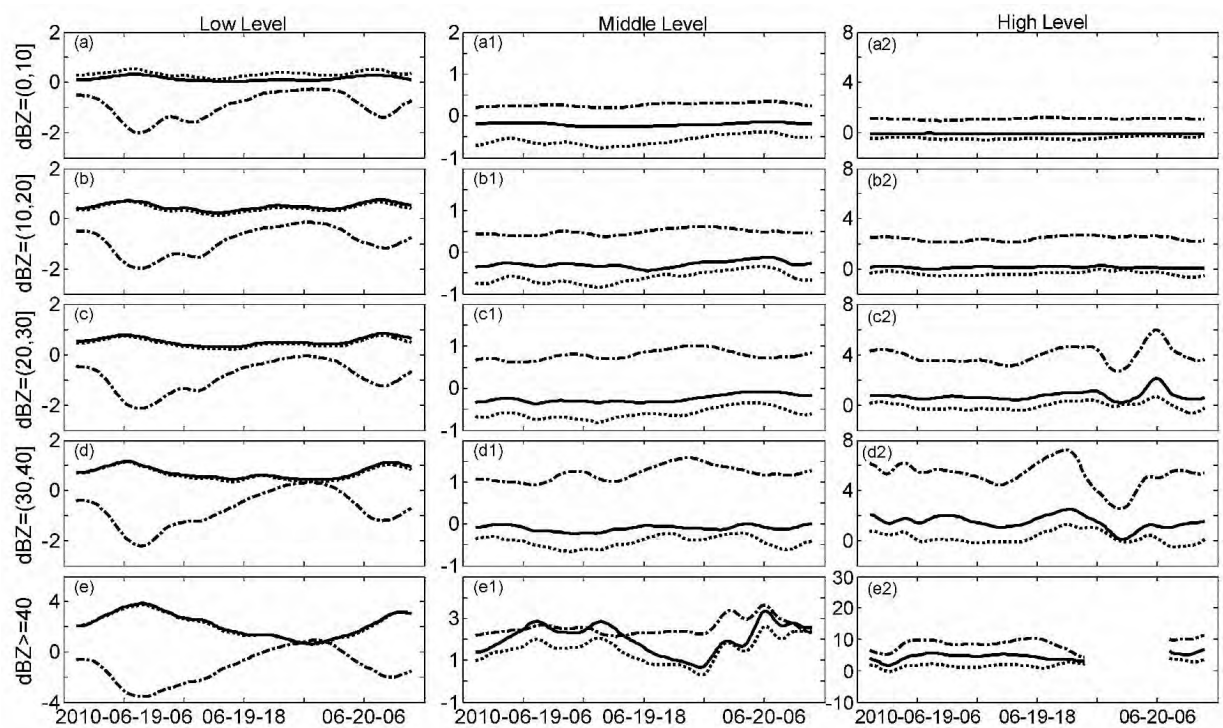

Figure 7. The average absolute errors of ω (solid line), ω_{qv} (dot-dash line) and ω_{ob} (dotted line) with respect to ω_{wrf} at each time point within dBZ intervals at low (a-e), middle (a1-e1) and high (a2-e2) levels. Units: Pa s^{-1}.

erage the three types of absolute errors were no longer overlapped, the absolute errors of ave_M_ω_{qv} and ave_M_ω with respect to ave_M_ω_{wrf} exhibited little difference within the (0,30] dBZ interval, the absolute error between ave_M_ω and ave_M_ω_{wrf} was closest to 0 within the (30,40] dBZ interval, and within the range of over 40 dBZ, the absolute error between ave_M_ω_{qv} and ave_M_ω_{wrf} was the largest, and the absolute error between ave_M_ω_{ob} and ave_M_ω_{wrf} was the smallest. In general, the vertical velocity obtained from the method disclosed herein was the most effective at the middle level.

At the high level, as shown in Fig.7a2-e2, the absolute error between ave_H_ω_{qv} and ave_H_ω_{wrf} was larger than the absolute errors of ave_H_ω and ave_H_ω_{ob} with respect to ave_H_ω_{wrf}, the absolute errors of ave_H_ω and ave_H_ω_{ob} with respect to ave_H_ω_{wrf} exhibited little difference; within the region where dBZ was relatively weak such as within the [0,20] dBZ range, the absolute error between ave_H_ω and ave_H_ω_{wrf} was smaller than the absolute error between ave_H_ω_{ob} and ave_H_ω_{wrf}, and vice versa when dBZ>=20. It was obvious that the method disclosed herein was also better than the wet Q-vector method at the high level, and was equally good as compared to the O'Brien method, whereas when it was above (20,40] dBZ, the O'Brien method was slightly better than the method disclosed herein.

It can be inferred from the above analysis that at the low level, the upward velocity values of ω and ω_{ob} were generally equal; moreover, the velocity value of ω was closer to ω_{wrf} as compared ω_{qv}. At the middle level, as compared to ω_{ob} and ω_{qv}, ω was closer to ω_{wrf} within each dBZ interval; at the high level, as compared to ω_{qv}, ω was closer to ω_{wrf} within each dBZ interval; As compared to ω_{ob}, except for that ω was closer to ω_{wrf} within the 0-10 dBZ range and the 10-20 dBZ range, as the dBZ increased, ω_{ob} was slightly better than ω.

With the same type of assessment performed on the downdraft (figure not shown), it is indicated that the results of downdraft were generally consistent with that of the updraft.

3.3 *All-level comparison*

Figure 8 showed the average vertical profile of the average upward and downward vertical velocities within varying dBZ intervals from 0000 UTC 19 June to 1200 UTC 20 June 2010. The data shown in the figure exhibited good consistency with the above analysis.

As shown in Fig.8, at 650-850 hPa, ω and ω_{ob} were generally overlapped regardless of either updraft or downdraft, and were closer to ω_{wrf} with respect to ω_{qv}; the intensity of ω and ω_{ob} were weaker than that of ω_{wrf}, whereas the intensity of ω_{qv} was remarkably stronger than that of ω_{wrf}; at 350-650 hPa, in the case of downdraft, the intensity of ω, ω_{ob} and ω_{qv} were all stronger than that of ω_{wrf}; in addition, ω was closest to ω_{wrf}, and ω_{ob} was farthest away from ω_{wrf}, with ω_{qv} lying somewhere in between; as for the updraft, at dBZ<40, the intensity of ω_{qv} was weaker than ω_{wrf}, and the intensity of ω and ω_{ob} were both stronger than ω_{wrf}; with respect to ω_{ob}, ω was closer to ω_{wrf}, and ω_{qv} and ω_{ob} were similar; when dBZ is >=40, the intensity of ω, ω_{ob} and ω_{qv} were all weaker than ω_{wrf}; meanwhile, ω and ω_{ob} were generally overlapped, and were closer to ω_{wrf} with respect to

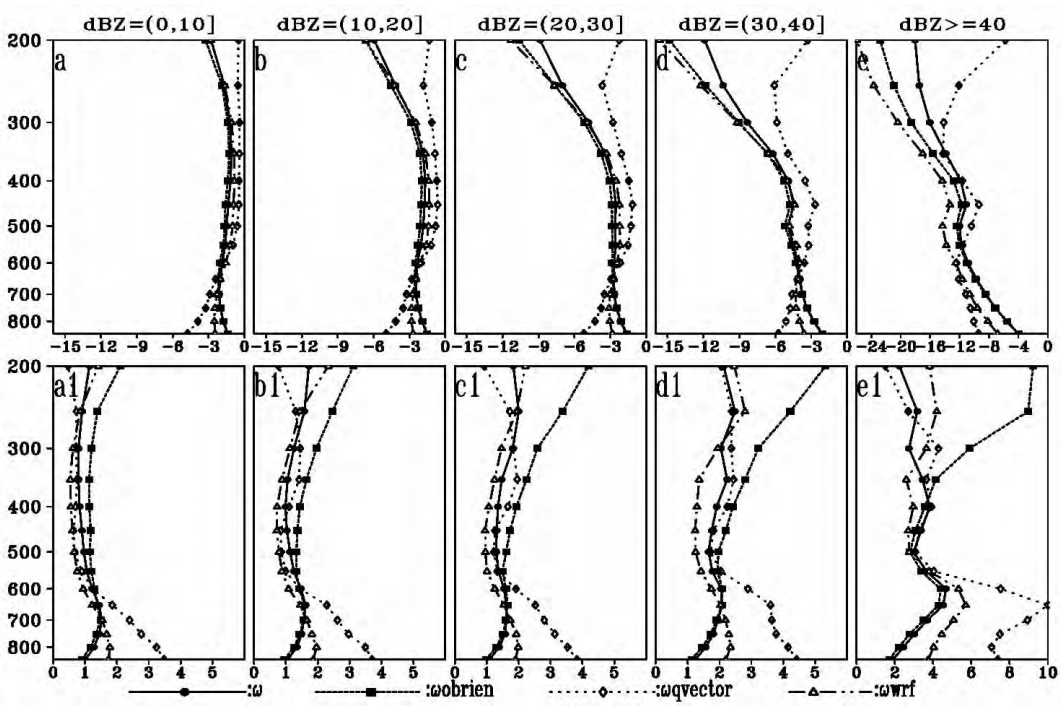

Figure 8. The average vertical profile of the average upward (a-e) and downward (a1-e1) velocities from 0000 UTC 19 June to 1200 UTC 20 June (Unit: Pa s^{-1}) ω (solid circle connected by solid lines), ω_{ob} (solid rectangle connected by dashed lines), ω_{qv} (hollow diamond connected by dotted lines) and ω_{wrf} (hollow triangle connected by dot-dash lines).

ω_{qv}; at 200-350 hPa, regarding the updraft, ω_{qv} was far away from ω_{wrf}, and ω_{ob} was closer to ω_{wrf} with respect to ω; regarding the downdraft, ω_{ob} was far away from ω_{wrf}, and ω was closer to ω_{wrf} with respect to ω_{qv}.

The ω_{qv} was significantly stronger than ω_{wrf} at the low level and was expressively weaker than ω_{wrf} at the high level possibly due to the result that ω_{qv} weighs more on the influence of water vapor. The vertical velocities obtained from each method individually exhibited relatively small error at the middle level; for the downward velocity, the error reached its peak at above 300 hPa. However, for the upward velocity, ω_{qv} had the largest error at above 300 hPa.

4 CONCLUSIONS

This article has provided a new method to obtain the Poisson's equation of the vertical shear and vertical velocity of the environmental wind from the continuity equations in a p coordinate system. The vertical velocity can be calculated by solving this Poisson's equation.

Furthermore, we compared the vertical velocity using the present method, with solutions from commonly used O'Brien method, ageostrophic wet Q-vector method, and the numerical simulation using WRF non-hydrostatic equilibrium mode (a MCC occurred from 0000 UTC 19 June to 1200 UTC 20 June 2010), and the following conclusions can be drawn from our work:

(1) The relationship between the horizontal vorticity and the vertical movement: when ω is in a fluctuating state, the vorticity of horizontal vorticity is proportional to $-\omega$. The updraft occurs when the vector of horizontal vorticity rotates counterclockwise, and the downdraft occurs when the said vector rotates clockwise.

(2) Using the vertical velocity from WRF model as reference and the calculations from O'Brien method and ageostrophic wet Q-vector method for comparison, we discovered that, overall, the present method is better than the other two in terms of the direction consistency, the absolute error, and the vertical profile of velocity. In general, better direction consistency can be achieved at a larger dBZ. As for the absolute error, all the three methods exhibit relatively large absolute errors at dBZ greater than 40, with the disclosed calculation method demonstrating a slightly better direction of the vertical velocity. It needs to be noticed that there is a certain level of error in terms of the numerical value of the vertical velocity for strong convection that is greater than 40 dBZ. However, the scale of dBZ shows little impact on the relative errors.

(3) The relationship between the horizontal vorticity and the vertical velocity remains when the vertical velocity reaches 10^1 m/s. It shows that the method disclosed herein can explain some mesoscale phenomena of vertical velocity within the range of 10^1 m/s.

Acknowledgement: We thank the SCMREX science team and office sponsored by Chinese Academy of Meteorological Sciences, Chinese Meteorological Administration for providing the observational data used in this paper. The data are available through application at. http://scmrex.cma.gov.cn.

REFERENCES:

[1] PANOFSKY H A. Methods of computing vertical motion in the atmosphere [J]. J Meteorol, 1946, 3: 45-49.
[2] GRAHAM R C. The estimation of vertical motion in the atmosphere [J]. Quart J Roy Meteorol Soc, 1947, 73:407.
[3] BALLEMY J C. Objective calculation of divergence, vertical velocity and vorticity [J]. Bull Amer Meteorol Soc, 1949, 30: 45-49.
[4] BANNON J K. The estimation of large-scale vertical currents from the rate of rainfall [J]. Quart J Roy Meteorol Soc, 1948, 74:57-67.
[5] PANOFSKY H A. Large-scale vertical velocity and divergence [J]. Compendium of Meteorology, 1951: 639-646.
[6] PETTERSSEN S. Weather Analysis and Forecasting [M]. Vol.1, New York: McGraw-Hill, 1956: 428pp.
[7] HALTINER G J, CLARKE L C, LAWNICAZAK G E J R. Computation of the large scale vertical velocity [J]. J Appl Meteorol, 1963, 2: 242-259.
[8] LV Mei-zhong, HOU Zhi-ming, ZHOU Yi. Dynamical Meteorology [M]. Beijing: China Meteorological Press, 2004: 99pp (in Chinese).
[9] O'BRIEN J J. Alternative solutions to the classical vertical velocity Problem [J]. J Appl Meteorol, 1970, 9: 197-203.
[10] LATEEF M A. Vertical motion, divergence, and vorticity in the troposphere over the Caribbean, August 3-5, 1963 [J]. Mon Wea Rev, 1967, 95: 778-790.
[11] FANKHAUSER J C. Convective processes resolved by a mesoscale rawinsonde network [J]. J Appl Meteorol, 1969, 8: 778-798.
[12] SMITH P J. An analysis of kinematic vertical motions [J]. Mon Wea Rev, 1971, 99: 715-724.
[13] HOSKINS B J, DRAGHICI I, DAVIES H C. A new look at the ω-equation [J]. Quart J Roy Meteorol Soc, 1978, 104: 31-38.
[14] YUE Cai-jun, SHOU Shao-wen, DONG Mei-ying. Quantitative Analysis of Several Q Vectors [J]. J Appl Meteorol Sci, 2003, 14(1): 39-48 (in Chinese).
[15] LARSEN M F, ROTTGER J. A comparison of thunderstorm reflectivities measured at VHF and UHF [J]. J Atmos Oceanic Technol, 1986, 4: 151-159.
[16] JAGANNADHA RAO V V M, NARAYANA RAO D, VENKAT RATNAM M, et al. Mean vertical velocities measured by Indian MST radar and comparison with indirectly computed values [J]. J Appl Meteorol, 2003, 42: 541-552.
[17] BROWNING K A, FOOTE G B. Airflow and hail growth in supercell storms and some implications for hail suppression [J]. Quart J Roy Meteorol Soc, 1976, 102: 499-533.
[18] FANKHAUSER J C. Thunderstorm-environment interactions determined from aircraft and radar observation [J]. Mon Wea Rev, 1971, 99: 171-192.
[19] MARWITZ J D. The structure and motion of severe hailstorms. Part I: Supercell storms [J]. J Appl Meteorol, 1972, 11: 166-179.
[20] PAN Xiao-bin, CHEN Jia-hua, WEI Shao-yuan. A numerical simulation of vertical wind shear influence on storm

cloud [J]. J Meteorol Sci, 1996, 16(2): 135-143 (in Chinese).
[21] WU Fei-yang, QU Nan, MA Hong-yun, et al. Analysis of vertical wind shear in severe convective storm on June 28, 2006 [J]. Meteorol Environ Sci, 2008, 31: 30-33 (in Chinese).
[22] YANG Da-sheng, JIAN Mao-qiu. The convective vertical velocity and the condensation heating [J]. Acta Sci Nat Univ Pekin, 1987, 1(1): 43-52 (in Chinese).
[23] ORLANSKI I. A rational subdivision of scales for atmospheric processes [J]. Bull Amer Meteorol Soc, 1975, 56: 527-530.
[24] CHARNEY J G. On the scale of atmospheric motions [J]. Geofysiske Publikasjoner, 1948, 17(2): 1-17.
[25] FUJITA T T. The downburst [M]// Satellite and Mesometeorology Research Project, University of Chicago, 1985: 122pp.
[26] GAO Shou-ting. Atmospheric Mesoscale Motion: Fundamentals of Dynamics and Forecasting Method [M]. Beijing: China Meteorological Press, 2007: 215pp (in Chinese).

Citation: DING Zhi-ying, ZHAO Xiang-jun, GAO Song et al. A novel method for calculating vertical velocity: A relationship between horizontal vorticity and vertical movement [J]. J Trop Meteorol, 2016, 22(2): 208-219.